Pergamon

Geochimica et Cosmochimica Acta, Vol. 66, No. 14, pp. 2603–2614, 2002

0016-7037/02 $22.00 + .00

PII S0016-7037(02)00860-8

Element partitioning between immiscible borosilicate liquids: A high-temperature centrifuge study

ILYA V. VEKSLER,[1] ALEXANDER M. DORFMAN,[2,3] DONALD B. DINGWELL,[2,4,2,5,*] and NIKOLAY ZOTOV[2,5]

[1]GeoForschungsZentrum Potsdam, Telegrafenberg B-120, D-14473 Potsdam, Germany
[2]Bayerisches Geoinstitut, Universität Bayreuth, D-95440 Bayreuth, Germany
[3]Vernadsky Institute of Geochemistry, Kosygin str., 19, 117975 Moscow, Russia
[4]IMPG Universität München, Theresienstrasse 41, D-80333 Munich, Germany
[5]Mineralogisch-Petrologisches Institut, Universität Bonn, D-53115 Bonn, Germany

(*Received May* 3, 2001; *accepted in revised form January* 14, 2002)

Abstract—The main objectives of this study were to investigate conditions for stable and metastable liquid immiscibility in dry borosilicate synthetic systems and to evaluate effects of temperature and bulk melt composition on two-liquid element partitioning and boron speciation. To distinguish between the stable immiscibility and quench heterogeneity, we used high-temperature centrifuge phase separation. For the case of stable liquid immiscibility, silica-rich (LS) and borate-rich (LB) conjugate liquids formed two distinct layers separated by a sharp meniscus. The liquids were quenched into glasses, which were analysed by electron microprobe. Some of the glasses were also studied by Raman spectroscopy. We used several synthetic mixtures along the danburite-anorthite ($CaB_2Si_2O_8$-$CaAl_2Si_2O_8$) and danburite-reedmergnerite ($CaB_2Si_2O_8$-$NaBSi_3O_8$) joins. In addition, we studied four complex, six-component, Mg-bearing compositions with variable Na_2O and Al_2O_3 contents. The experiments show that the width of the LS-LB miscibility gap decreases more rapidly with the B-Al substitution (in the danburite-anorthite join) than with the Ca-Na substitution, implying that interactions between network-forming elements have a greater effect on borate-silicate unmixing than the nature of network-modifying cations. Ca and Mg partition strongly to the depolymerised borate-rich liquid with LB-LS partition coefficients of ~40 and higher. On the other hand, two-liquid partition coefficients of Na and Al in most cases are close to 1 and show complex variations with temperature and bulk melt composition. Raman spectra of LB glasses quenched at different temperatures suggest that the proportion of trigonal boron in bulk boron content decreases with decreasing temperature. The change in boron speciation appears to affect Al and Na two-liquid partitioning in such a way that at low temperatures, the latter element becomes more compatible with LS.

1. INTRODUCTION

Boron plays a complex and unique role in the structure of borosilicate melts and glasses. It is the smallest of the network-forming cations with a high ionic charge, and it forms two distinct structural units: BO_3 triangles (similar to CO_3 carbonate groups) and BO_4 tetrahedra (similar to the main building blocks of silicate and aluminosilicate structures: SiO_4 and AlO_4 units) (see review by Dingwell et al., 1996). Both trigonal and tetrahedral units tend to polymerise and form numerous combinations with each other, SiO_4, AlO_4, and other network-forming components. Boron produces strong effects on the physical and chemical properties of melts (Dingwell et al., 1996) and therefore has broad applications in the glass industry (e.g., Scholze, 1988).

Because of its low natural abundances in most magmatic systems, boron is usually a trace element. Boron abundance in the upper mantle is estimated to be around 0.1 ppm (Leeman and Sisson, 1996). In igneous systems, boron behaves as an incompatible trace element. It is mobilised by melts and to an even larger extent by aqueous fluids, in which it is highly soluble at medium to high temperatures. It is concentrated in marine sediments, especially in evaporites. Thus, one might expect crustal anatectic melts produced by remelting of boron-rich metasediments to have the highest boron contents among the other natural silicate liquids. Some S-type granites are indeed enriched in boron, and highly evolved peraluminous rhyolitic obsidian may contain as much as 0.6 wt.% B_2O_3 (Pichavant et al., 1988). It is important to note that because of the high mobility of boron in hydrothermal fluids, bulk rock analyses of granitic rocks, especially their deeper plutonic varieties, are not likely to represent boron concentrations in parental melts (London et al., 1996).

Recently, natural silicic melts with up to a few weight percent of B_2O_3 have been identified in studies of melt inclusions in minerals from granitic pegmatites (Thomas et al., 2000). Reexamination of fluid inclusions in tourmaline-bearing pegmatites has revealed that sassolite (H_3BO_3) is an abundant daughter phase, and bulk boric acid concentrations in the pegmatitic fluids have been estimated to vary from 2 to 26 wt.% (Peretyazko et al., 2000). This discovery confirms that fractionation of magmatic fluids may account for boron escape from evolved granitic melts and explains why the vast majority of plutonic rocks are lower in boron than their volcanic analogues (London et al., 1996). Apparently, high concentrations of B_2O_3 can be retained in fully crystalline igneous rocks only if boron has been fixed in B-rich minerals, such as tourmaline or danburite.

These recent observations underline the fact that experimental investigation of liquid immiscibility in borosilicate systems may have important applications for magmatic and magmato-

* Author to whom correspondence should be addressed (veksler@gfz-potsdam.de).

Table 1. Starting bulk compositions (nominal, wt.%).

	SiO_2	B_2O_3	Al_2O_3	MgO	CaO	Na_2O	Total
CBS	48.88	28.32	—	—	22.81	—	100
NCMBAS-5	49.57	27.00	1.26	0.88	20.53	0.77	100
NCMBAS-10	50.10	25.58	2.52	0.88	19.39	1.53	100
NCMBAS-20	51.16	22.75	5.04	0.88	17.11	3.07	100
NCBS	61.07	21.23	—	—	11.40	6.30	100
NC3BS	54.97	24.77	—	—	17.10	3.15	100
CB7AS	48.08	24.38	5.10	—	22.44	—	100
CB13A3S	47.70	22.45	7.59	—	22.26	—	100
CB3AS	47.32	20.56	10.04	—	22.08	—	100
CBAS	45.86	13.28	19.46	—	21.40	—	100

hydrothermal petrogenesis, as has long been the case for material sciences. Liquid immiscibility is the most vivid manifestation of nonideal mixing and is a common phenomenon in borosilicate systems (Scholze, 1988). The study of coexisting immiscible liquids provides both a macroscopic means to evaluate the energetics and relative stability of chemical bonds in silicate melts and also insight into their structure and speciation on a microscopic level.

In this paper, we present new experimental data for the two-liquid partition coefficients of major components in borosilicate systems. The relatively high viscosity of the polymerised melts is an obstacle for phase separation at high temperature, and thus, distinguishing between metastable (quench) heterogeneity and equilibrium liquid immiscibility presents a significant challenge. The utilisation of a high-temperature centrifuge separation in this study enabled us to separate immiscible liquids into distinct layers at high temperature and thereby to distinguish clearly between droplets that existed at run temperature from those that nucleated during quenching.

2. BACKGROUND

One of the most striking and fundamental features of borosilicate melts revealed by previous experimental studies of dry synthetic systems is a tendency of the B_2O_3-rich liquids toward stable and metastable unmixing. In its simplest case, such behaviour is observed on the SiO_2-B_2O_3 join (Levin et al., 1964; Rockett and Forster, 1965; Dingwell et al., 1996), where a pronounced S-shaped solidus of silica polymorphs indicates a metastable, subsolidus immiscibility dome hidden within the quartz + liquid stability field. Ternary systems with alkali oxides M_2O-B_2O_3-SiO_2 (M = Li, Na, K) are also characterised by regions of metastable liquid immiscibility (Haller et al., 1970). In contrast, borosilicate ternary systems with oxides of divalent elements such as alkaline earths (MgO, CaO, BaO), PbO, and ZnO have broad fields of stable liquid immiscibility stretching from the B_2O_3-SiO_2 bounding join into the ternary system (Levin et al., 1964). The broad two-liquid fields are often crossed by cotectics (e.g., in the CaO-B_2O_3-SiO_2 system), and thus, the immiscible liquids may be saturated either by silicate or borate mineral phases, depending on the SiO_2-B_2O_3 ratio of bulk compositions.

Relationships between the metastable and stable liquid immiscibility in more complex, multicomponent systems have not been widely studied. We have found no previous publications on element partitioning between the immiscible liquids in borosilicate systems with more than three components.

Borosilicate glasses, especially those used in industry, have been studied extensively by various spectroscopic methods, especially nuclear magnetic resonance (NMR) and Raman spectroscopy (see review by Dingwell et al., 1996). Solution calorimetry has also been used to study boron speciation and energetics of chemical bonds in borate and borosilicate melts and glasses. Geisinger et al. (1988) performed the calorimetric study of glasses along the reedmergnerite-albite ($NaBSi_3O_8$-$NaAlSi_3O_8$) join combined with NMR spectroscopy (^{11}B, ^{23}Na, ^{27}Al, and ^{29}Si). Solution calorimetry has revealed a positive enthalpy of mixing along the join, which suggests that Al and B do not substitute ideally for each other and that clustering occurs on a microscopic scale. The clusters are likely to be regions rich in trigonal BO_3 groups coexisting with more silica-rich network regions. No macroscopic evidence for metastable phase separation has been found in the glasses.

3. EXPERIMENTAL AND ANALYTICAL METHODS

The basic composition used in this study (CBS; Table 1) has a bulk stoichiometry of the mineral danburite ($CaB_2Si_2O_8$) and is located close to the centre of the two-liquid field of the CaO-B_2O_3-SiO_2 ternary system (Morey and Ingerson, 1937; Levin et al., 1964). To study the effects of Na-Ca and Al-B substitution on the two-liquid phase separation, we prepared a series of compositions along the danburite-reedmergnerite ($CaB_2Si_2O_8$-$NaBSi_3O_8$) and danburite-anorthite ($CaB_2Si_2O_8$-$CaAl_2Si_2O_8$) joins. We also studied three six-oxide compositions (NCMBAS) along the $CaB_2Si_2O_8$-$NaAlSi_2O_6$ join with the addition of 0.88 wt.% MgO. The starting compositions were prepared by mixing reagent-grade H_3BO_3, SiO_2, Al_2O_3, MgO, $CaCO_3$, and Na_2CO_3, sintering the mixtures at 950°C until constant weight (to ensure complete removal of H_2O and CO_2), and then grinding and fusing them repeatedly (two or three times) at 1300°C. Bulk compositions of the experimental charges and run conditions are listed in Tables 1 and 2.

Fine-grained powders of the sintered mixtures were loaded into Ni or Pt cylindrical containers, 5 to 6 mm in diameter and approximately 10 mm long, then melted and centrifuged at atmospheric pressure and 900 to 1350°C. The runs were performed in a small, cylindrical, wire-wound electric furnace mounted on a centrifuge (for details of the experimental equipment and techniques, see Dorfman et al., 1996). Because of the high viscosity of the borosilicate liquids, centrifuge separation

Table 2. Run conditions and run products. Run products with distinct layers or globules of immiscible liquids are listed as *LB + LS*. Opaque, turbid glasses are listed as *LBS* and were interpreted as products of metastable phase separation. *L* stands for clear, transparent, homogeneous glasses.

Run	Starting composition	T (°C)	Acceleration g (g = 9.8 m/s^{-2})	Duration (h)	Run products
98-004	CBS	1250	1000	1	LB + LS
98-006	NCMBS-5	1250	1000	3	LB + LS
98-007	NCMBS-10	1250	1000	3	LB + LS
98-008	NCMBS-20	1250	1000	3	LB + LS
98-015	NCMBS-10	1300	1000	3	LB + LS
98-016	NCBS	1150	1000	3	LBS
98-017	CBAS	1150	1000	3	L
98-018	NCBS	1000	1000	3	LB + trace LS
98-019	CBAS	1000	1000	3	L
98-020	NCBS	900	1000	3	LB + trace LS
98-021	NC3BS	1250	1000	3	LB + LS
98-022	CB3AS	1250	1000	3	LBS
98-024	CB3AS	1150	1000	3	LB + LS
98-025	NC3BS	1150	1000	3	LB + LS
98-026	NCMBS-20	1050	1000	3	LB + LS
98-027	NCMBS-20	1150	1000	3	LB + trace LS
98-028	NCMBS-10	1050	1000	3	LB + LS
98-029	NCMBS-10	1150	1000	3	LB + LS
98-030	NC3BS	1050	1000	3	LB + LS
98-031	NCMBS-20	950	1000	3	LB + LS
98-032	NCMBS-20	1250	1000	3	LB + LS
98-033	NCMBS-20	1050	1000	3	LB + LS
98-034	NCMBS-20	1150	1000	3	LB + LS
98-040	CB7AS	1150	1000	1	LB + LS
98-041	CB7AS	1050	1000	3	LB + LS
98-042	CB7AS	1250	1000	1	LB + LS
98-043	CB13A3S	1150	1000	1	LB + LS
98-044	CB13A3S	1250	1000	1	LB + trace LS
98-045	CBS	1350	1	1.5	LB + LS
98-046	CBS	1250	1	1.5	LB + LS
98-047	CBS	1150	1	2.5	LB + LS
98-048	CBS	1050	1	3.5	LB + LS
98-054	CB13A3S	1050	1000	3	LB + LS
98-055	CB13A3S	1300	1000	1	LB + LS

was performed for long run durations (up to 3 h) and at the maximum acceleration of 1000g (g = 9.8 m/s^2). Quenching was achieved in air by turning the electric furnace off while the centrifuge rotation continued. Typically, 2 min were required to cool the furnace down to room temperature. We believe that quenching rates were adequate because we did not find quench crystal phases, nor indications of significant secondary separation of the immiscible liquids during quenching. After the runs, the containers with quenched glasses were cut lengthwise into two halves. One part was mounted in epoxy and used for electron microprobe analyses. The other halves were kept for optical examination and other purposes. Charges used in this study proved to be stable in air, even at high temperatures and in open containers. No measurable volatility was detected by weight loss.

Immiscible layers and globules were analysed twice by Cameca SX-50 microprobes in two laboratories using different analytical procedures and standards. Preliminary pilot analyses were performed at Bayerisches Geoinstitut (BGI), Bayreuth. The glasses were analysed in wavelength-dispersive spectroscopy mode at 10 kV accelerating voltage and 30 nA beam current. PC-3 LSM crystal and 60 s counting time were used for boron determination. Pure elemental B was a primary standard, and a synthetic haplogranite glass with 19 wt.% B_2O_3 (HPG8B19; Dingwell et al., 1992) was used as a secondary standard for further calibration. To check and improve the electron microprobe results, the samples were reanalysed at GeoForschungsZentrum (GFZ) Potsdam with a PC-2 crystal for light elements, 10 kV accelerating voltage, 30 nA beam current, and an anticontamination cold trap cooled with liquid N_2. In the second round of analyses, LaB_6 was a primary standard for B, and four additional standards with variable B contents (natural danburite and three synthetic glasses, including HPG8B19) were used to test and improve the calibration. Comparison of the two data sets revealed a good agreement for all the elements except Si and B. Boron appeared to be systematically overestimated by a factor of 1.06 to 1.08 in the first data set, and the final results listed in Table 3 are based mostly on the data from the laboratory at GFZ Potsdam.

Raman studies were carried out at the BGI using the 514.5-nm line of a coherent Ar+ laser used as an excitation source operating at 1 ± 0.1 W power. Unpolarised measurements were done with a Dilor XY triple spectrometer equipped with an 1800-gr/mm holographic grating and a charge-coupled device detector cooled by liquid N_2. The measurements were performed in backscattering geometry under an Olympus microscope with 100× objective using confocal entrance optics (confocal hole of 800 μm) in multiwindow mode. The measuring time was 120 s per spectral window. A constant back-

Table 3. Electron microprobe analyses of immiscible boron-rich liquids (LB) and silica-rich liquids (LS) in wt.% an two-liquid partition coefficients calculated as mole ratios: $D = {}^{LB}X_i/{}^{LS}X_i$..

Sample	Starting mix.	T (°C)	Phase	SiO_2	Al_2O_3	B_2O_3	MgO	CaO	Na_2O	Total
98-0044	CBS	1250	LB	35.88	0.05	33.25	0.21	30.94	0.01	100.35
			LS	78.07	0.01	20.72	0.41	0.66	0.01	99.49
			D	0.47	—	1.64	—	47.84	—	
98-006	NCMBAS-5	1250	LB	38.93	1.89	31.13	1.31	25.97	1.01	100.24
			LS	79.30	0.26	18.95	0.06	0.54	0.28	99.38
			D	0.50	7.49	1.66	21.11	48.24	3.68	
98-007	NCMBAS-10	1250	LB	45.79	3.19	27.79	1.17	21.15	1.79	100.87
			LS	78.75	0.67	17.86	0.12	1.26	0.61	99.28
			D	0.58	4.73	1.55	9.37	16.72	2.91	
98-008	NCMBAS-20	1250	LB	50.35	5.31	23.99	0.97	16.46	3.04	100.12
			LS	66.40	4.02	18.92	0.53	7.45	2.79	100.11
			D	0.76	1.33	1.27	1.84	2.22	1.09	
98-015	NCMBAS-10	1300	LB	45.34	3.07	28.77	1.22	21.15	1.73	101.28
			LS	80.05	0.62	17.48	0.08	0.80	0.54	99.57
			D	0.56	4.91	1.63	15.75	26.25	3.17	
98-021	NC3BS	1250	LB	48.39	0.03	25.86	0.09	21.85	3.70	99.91
			LS	82.22	0.01	15.30	0.01	1.07	0.71	99.32
			D	0.59	1.95	1.70	6.99	20.53	5.28	
98-024	CB3AS	1150	LB	47.89	9.27	19.94	0.06	22.43	0.06	99.65
			LS	85.90	0.83	13.27	0.00	0.98	0.03	101.00
			D	0.58	11.65	1.57	—	23.96	—	
98-025	NC3BS	1150	LB	45.64	0.02	28.23	0.09	23.36	3.46	100.80
			LS	82.14	0.02	15.05	0.00	1.44	0.68	99.33
			D	0.55	—	1.86	—	16.04	5.07	
98-026	NCMBAS-20	1050	LB	49.11	5.10	24.41	1.08	18.29	3.00	100.98
			LS	72.05	4.50	15.78	0.26	3.78	2.99	99.37
			D	0.67	1.12	1.53	4.08	4.78	0.99	
98-028	NCMBAS-10	1050	LB	38.79	3.44	29.29	1.50	26.05	1.85	100.92
			LS	81.77	2.00	15.30	0.04	0.83	1.09	101.04
			D	0.48	1.73	1.94	36.37	31.83	1.72	
98-029	NCMBAS-10	1150	LB	43.56	3.36	27.18	1.25	23.86	1.81	101.00
			LS	80.13	1.47	15.40	0.07	1.22	0.84	99.14
			D	0.54	2.27	1.76	16.85	19.41	2.15	
98-030	NC3BS	1050	LB	41.11	0.02	29.21	0.10	25.43	3.90	99.78
			LS	85.43	0.03	11.73	0.00	0.56	0.44	98.20
			D	0.47	—	2.44	—	44.92	8.67	
98-032	NCMBAS-20	1250	LB	49.00	5.15	23.31	0.96	18.65	3.04	100.10
			LS	69.21	3.93	17.76	0.47	6.62	3.00	100.99
			D	0.72	1.33	1.34	2.07	2.87	1.03	
98-034	NCMBAS-20	1150	LB	48.67	5.05	23.86	0.87	18.79	2.96	100.19
			LS	68.09	4.02	17.38	0.31	6.69	2.89	99.38
			D	0.71	1.25	1.37	2.78	2.80	1.02	
98-033	NCMBAS-20	1050	LB	46.94	5.28	23.07	0.85	20.04	3.00	99.17
			LS	74.3	4.19	15.62	0.15	2.84	2.81	99.92
			D	0.65	1.29	1.51	5.89	7.22	1.09	
98-031	NCMBAS-20	950	LB	45.08	5.03	23.93	0.84	21.68	2.99	99.55
			LS	68.18	5.13	17.87	0.11	7.01	3.54	101.84
			D	0.69	1.02	1.39	8.04	3.21	0.87	
98-040	CB7AS	1150	LB	38.84	5.83	26.95	0.00	28.90	0.03	100.55
			LS	81.40	0.34	17.60	0.00	0.80	0.01	100.15
			D	0.49	17.79	1.58	—	37.52	—	
98-041	CB7AS	1050	LB	37.00	6.02	26.93	0.00	29.54	0.02	99.52
			LS	80.29	0.36	17.02	0.01	0.96	0.03	98.68
			D	0.47	17.15	1.63	—	31.66	—	
98-042	CB7AS	1250	LB	42.95	5.76	25.13	0.00	26.46	0.02	100.33
			LS	78.52	0.64	17.33	0.01	1.73	0.02	98.25
			D	0.56	9.09	1.47	—	15.57	—	
98-043	CB13A3S	1150	LB	43.55	8.01	24.52	0.00	24.83	0.03	100.94
			LS	78.94	0.39	18.15	0.00	1.05	0.02	98.55
			D	0.56	20.88	1.37	—	24.06	—	
98-044	CB13A3S	1250	LB	39.58	8.50	23.92	0.00	26.92	0.03	98.95
			LS	79.84	0.49	17.81	0.00	1.10	0.03	99.26
			D	0.52	18.38	1.41	—	25.77	—	
98-045	CBS	1350	LB	36.52	0.08	33.15	0.06	30.55	0.01	100.36
			LS	81.47	0.00	17.47	0.00	0.47	0.01	99.42
			D	0.45	—	1.91	—	65.90	—	

(*continued*)

Table 3. (*continued*)

Sample	Starting mix.	*T* (°C)	Phase	SiO_2	Al_2O_3	B_2O_3	MgO	CaO	Na_2O	Total
98-046	CBS	1250	LB	32.36	0.02	34.35	0.04	33.83	0.01	100.60
			LS	81.45	0.01	18.18	0.00	0.52	0.01	100.17
			D	0.40	—	1.92	—	66.79	—	
98-047	CBS	1150	LB	31.15	0.05	34.00	0.04	34.96	0.00	100.20
			LS	81.53	0.02	17.89	0.01	0.11	0.02	99.56
			D	0.39	—	1.94	—	336.89	—	
98-048	CBS	1050	LB	29.13	0.02	34.86	0.04	36.08	0.01	100.13
			LS	80.77	0.01	18.41	0.01	0.68	0.01	99.90
			D	0.37	—	1.94	—	54.32	—	

ground was then subtracted from the experimental spectra, and they were Fourier smoothed.

4. RESULTS

4.1. Run Products

In cases of stable, macroscopic liquid immiscibility, high-temperature centrifuge separation resulted in the formation of two distinct layers separated by a sharp meniscus. The silica-rich liquid (LS) was of lower density and accumulated on top of the borate-rich melt (LB). Examples of the quenched centrifuged charges are shown in Figure 1. In some runs, melt viscosities (especially those of LS) were too high and run durations were not long enough to achieve full separation. In those cases, globules of LB persisted in the upper layer of LS after the quench. The size of the globules varied from several microns to several hundred microns, and a close look at them reveals that the globules did not nucleate during quench but were present for quite some time during the run and were moving slowly down through LS (Fig. 2). Those immiscible charges that were not centrifuged produced numerous evenly dispersed globules and no signs of gravitational phase segregation. The LB usually quenched to whitish, opaque glasses, which are believed to be an indication of microscopic, colloidal phase separation, presumably a quenching phenomenon.

Those compositions that did not produce the two-layer phase separation formed very similar opaque glasses, with the signs of suboptical heterogeneity, which were interpreted as metastable, quench liquid immiscibility. Such products are listed in Table 2 as LBS charges. The only composition that produced clear, transparent glass was the CBAS mixture on the danburite-anorthite join with 50 mol.% of each component.

In Figure 1, a series of thin sections illustrates how the run products change as the bulk composition of charges approaches the border of a miscibility gap. With increasing Na_2O and Al_2O_3 contents, the proportion of LS decreases; so does the viscosity of LS. This results in turn in a better phase separation and disappearance of LB globules from the LS layer.

4.2. Compositions of Conjugate Liquids

Electron microprobe data on the immiscible liquids LS and LB are listed in Table 3. The table also includes partition coefficients of major elements between the conjugate liquids. Several representative tie lines are plotted in Figures 3 and 4. The projections demonstrate that on the alkali-free joins, the LS is composed mainly of SiO_2 and B_2O_3, whereas concentrations

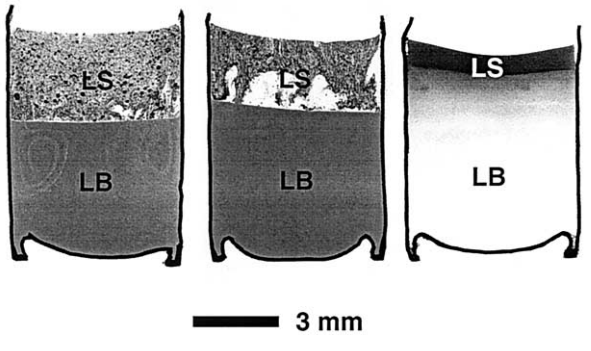

Fig. 1. Thin sections of the products of high-temperature centrifuge separation at 1250°C. The starting bulk compositions with increasing Na_2O and Al_2O_3 contents (from left to right) are NCMBAS-5, NCMBAS-10, and NCMBAS-20. The samples are listed in Tables 2 and 3 as 98-006, 98-007, and 98-008. The capsules are cut lengthwise along the vertical axis. Borate-rich liquid (LB) forms a lower, denser layer, and some unseparated globules remain in the silicate-rich liquid (LS).

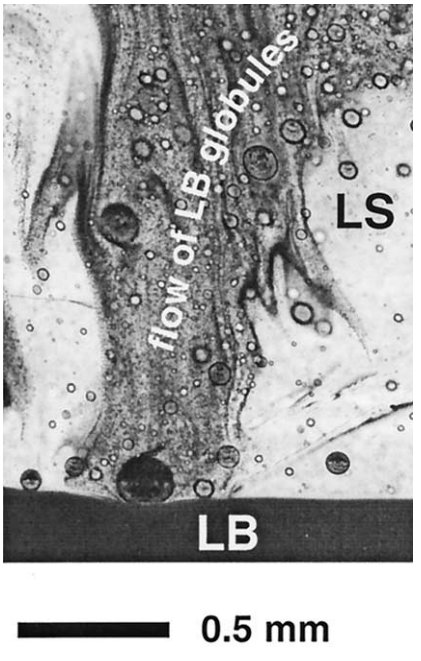

Fig. 2. A close-up of the interface between silicate-rich liquid (LS) and borate-rich liquid (LB) in the middle sample of Figure 1, which shows the globules of LB moving through LS.

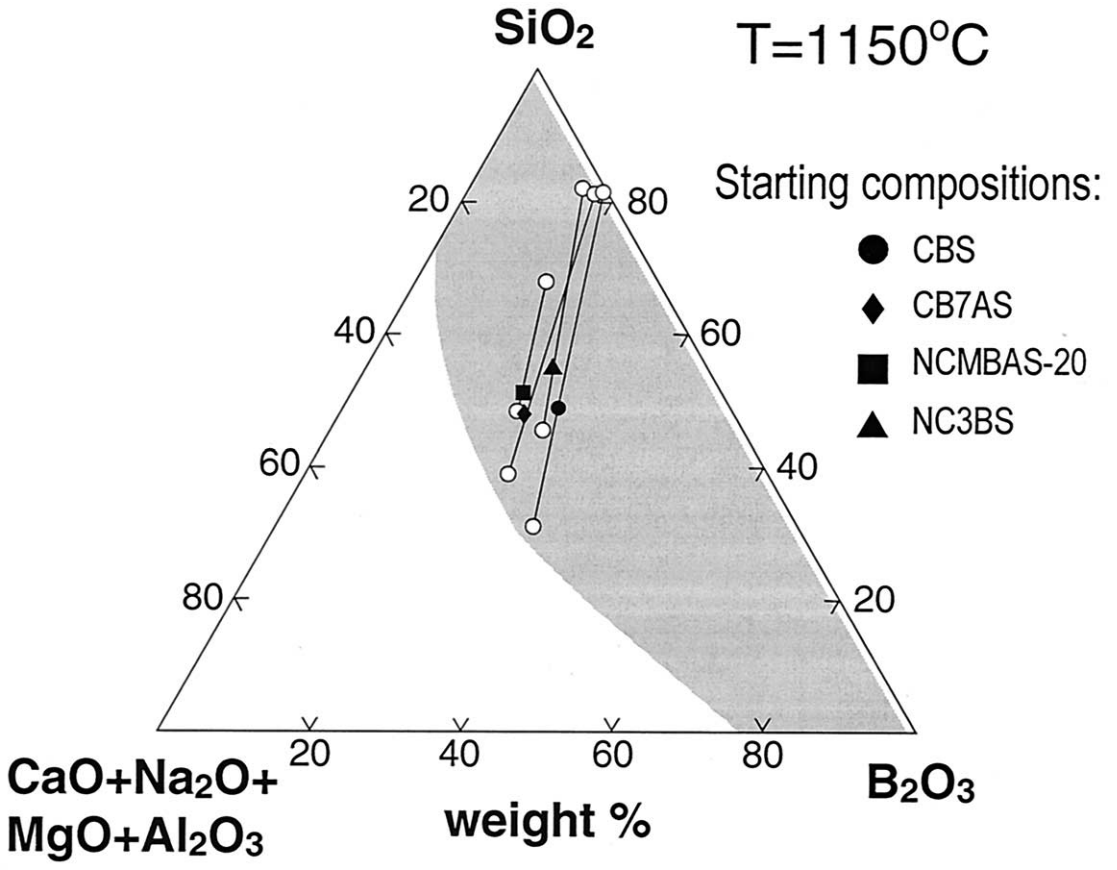

Fig. 3. Projection of selected tie lines onto the $CaO-B_2O_3-SiO_2$ ternary diagram. Grey shaded field shows the extent of the two-liquid field in the $CaO-B_2O_3-SiO_2$ system. All the experimental tie lines are at 1150°C.

of other oxides are low. Thus, the compositions of LS lie very close to the $SiO_2-B_2O_3$ bounding join (Fig. 3). Al-B substitution in the danburite ternary composition along the $CaB_2Si_2O_8$-$CaAl_2Si_2O_8$ join has virtually no effect on the composition of LS (Fig. 4a), and almost all the aluminium stays in LB. In contrast, the addition of Na_2O has a significant effect on the composition of LS (Figs. 4b and 4c). Concentration of B_2O_3 in LS decreases, while solubilities of other oxides increase and the miscibility gap shrinks. In all joins studied, the liquid immiscibility region decreases also with increasing temperature, as illustrated, for example, by two isotherms in Fig. 4c. It should be noted that in Na-bearing joins, LS-LB tie lines remain subparallel to the $CaB_2O_4-SiO_2$ bounding join (Figs. 4b and 4c), indicating almost equal concentration of $NaBO_2$ or $NaAlO_2$ components in both coexisting liquids.

4.3. Raman Results

Raman spectra of the immiscible liquids were obtained for two samples (98-045 and 98-046) with the bulk danburite composition. We chose the basic three-component composition to avoid additional complications in the interpretation of Raman spectra. To achieve higher quenching rates and better correspondence between melts and glasses, the samples were not centrifuged and after 1.5 h at 1350 and 1250°C were quenched in water.

4.3.1. Silica-rich glass

The Raman spectra of the silica-rich phase LS in both samples are similar (Fig. 5a), showing no dependence on the quenching temperature. The spectra of LS are very similar to the Raman spectrum of pure amorphous SiO_2 (a-SiO_2), which indicates that the LS is highly polymerised and B_2O_3 is present mostly as a glass former rather than a glass modifier. This conclusion is further supported by the fact that the intensity of the broad band at ~1400 cm^{-1}, commonly attributed to BO_3 units (see, e.g., Furukawa and White, 1981; Chryssikos et al., 1994), is relatively small compared to the Si-O bands. Moreover, it has been found that BO_3 units linked to BO_4 tetrahedra exhibit B-O stretching vibrations at lower frequencies (Chryssikos et al., 1994, and references therein). Thus, the presence of a peak around 1380 cm^{-1} would imply that some of the BO_3 units are linked to BO_4 tetrahedra.

Despite their general similarity, there are important differences between the Raman spectra of the investigated silica-rich borosilicate glasses and a-SiO_2. The peak at ~440 cm^{-1}, which is commonly assigned to in-plane Si-O-Si bending vibrations (McMillan, 1984), is shifted to higher frequencies (463 cm^{-1}), which indicates that the average Si-O-Si bond angle is smaller in the LS glasses. This probably results from the formation of Si-O-B linkages, because ab initio molecular orbital calculations (Gibbs, 1982, and references therein) have

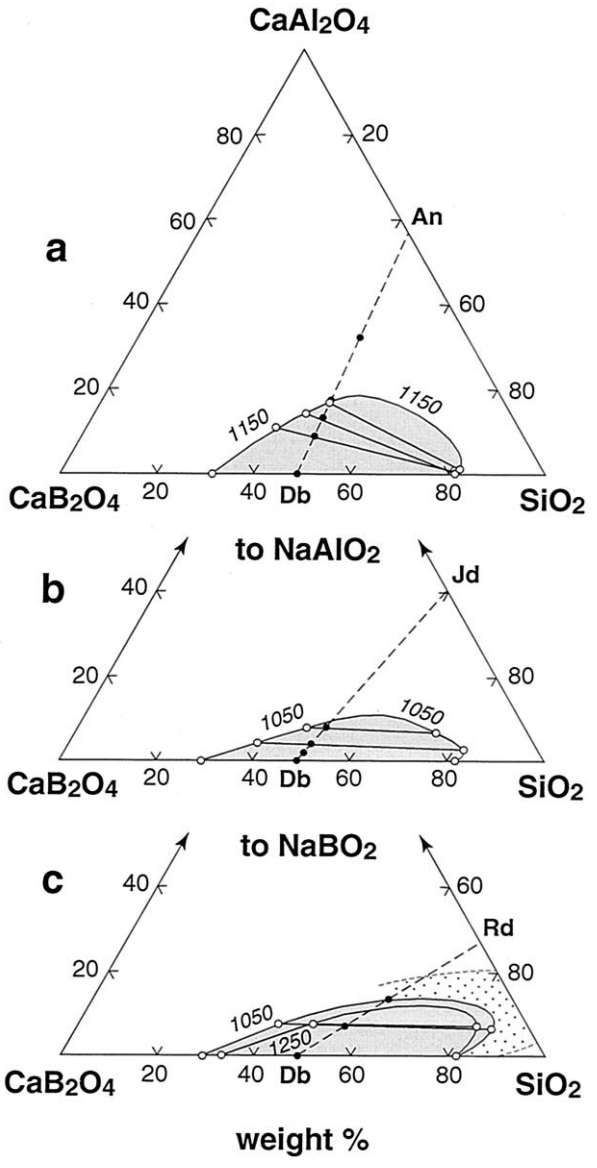

Fig. 4. Pseudoternary projections showing the regions of stable and metastable liquid immiscibility and representative silicate-rich liquid (LS)–borate-rich liquid (LB) tie lines. (a) The danburite-anorthite join. (b) The danburite-jadeite join. (c) The danburite-reedmergnerite join. Grey shaded fields show the regions of stable liquid immiscibility within the specified isotherms; dotted area corresponds to region of metastable immiscibility. White circles connected with tie lines correspond to the LS and LB conjugate compositions; black circles correspond to the starting compositions. An = $CaAl_2Si_2O_8$; Db = $CaB_2Si_2O_8$; Jd = $NaAlSi_2O_6$; Rd = $NaBSi_3O_8$.

clearly shown that the minimum energy Si-O-B angle is significantly smaller than the minimum energy Si-O-Si angle (126 and 142°, respectively). The intensity of the sharp peak at ~600 cm^{-1} in the a-SiO_2 spectra, commonly assigned to planar three-membered rings (Galeener, 1982), is present only as a weak shoulder. The sharp peak at ~495 cm^{-1}, commonly attributed to planar four-membered rings (Galeener, 1982), is completely missing in the spectra of the LS. In other words, the incorporation of boron into the LS liquid leads to a change in the ring distribution (medium-range order). New weak bands at ~675 and 750 cm^{-1} are observed, which some authors interpret as evidence for the presence of six-membered borate rings built of both BO_4 and BO_3 units (Konijnendijk and Stevels, 1975; Furukawa and White, 1981).

The peak at ~800 cm^{-1}, which arises from complex motion of Si atoms against the bridging oxygens (McMillan, 1984; Zotov et al., 1999), is weaker in the borosilicate glasses and becomes more symmetric, suggesting some degree of depolymerisation. This conclusion is further confirmed by the increased intensity of the high-frequency bands at 930 and 1050 cm^{-1}, which is commonly attributed to the presence of non-bridging oxygens (see below). The increase of the Raman intensity of the 930 cm^{-1} band, however, is at least partially due to the presence of BO_4 tetrahedra (Furukawa and White, 1981).

In conclusion, the structure of the LS, determined from the Raman spectroscopic study, is of a polymerised network built of SiO_4 and BO_4 tetrahedra with some BO_3 units attached to BO_4 tetrahedra.

4.3.2. Borate-rich glass

The Raman spectra of the LB glasses are quite different (Fig. 5b) but are comparable to the spectra of depolymerised CaO-SiO_2 (Mysen et al., 1980) and SiO_2-$CaAl_2O_4$ (Seifert et al., 1982) glasses. The Raman intensity below 400 cm^{-1} and of the high-frequency bands at ~970 and 1060 cm^{-1} is much higher than in the silica-rich glasses. These features clearly indicate that the LB glasses are strongly depolymerised. In binary alkali- and alkaline-earth glasses, the band at ~930 to 950 cm^{-1} is assigned to Q^2 units (where Q^n denotes a tetrahedron with *n* bridging oxygens), while the peak at ~1100 cm^{-1} is assigned to Q^3 units (McMillan, 1984). Therefore, the Raman data suggest that LB glasses contain mainly Q^2 and Q^3 species. However, the presence of ~33 to 34 wt.% B_2O_3 (Table 3) makes the quantification of the Q-species distribution in borosilicate glasses more difficult because, as already mentioned, the presence of BO_4 units also gives rise to Raman bands in the range 930 to 950 cm^{-1}.

The intensity of the band at ~1460 cm^{-1} is also much higher than in the Raman spectra of the LS glasses, which clearly indicates that a significant part of B_2O_3 is present as BO_3 units. Besides that, this peak is quite symmetric, which indicates that the proportion of BO_3 units linked to BO_4 tetrahedra is relatively small. Nevertheless, we cannot exclude the presence of some BO_4 units incorporated in the silicate network. This is indirectly confirmed by the fact that the intensity of the high-frequency peak at ~1100 cm^{-1} is weaker than in pure CAS glasses (Mysen et al., 1980).

Some subtle differences are also observed between the spectra of glasses quenched from different temperatures. In particular, our data suggest a higher concentration of BO_3 units in glasses quenched from higher temperature (sample 98-045) and that the structure is slightly less depolymerised. The decrease in the proportion of tetrahedral boron with increasing temperature has been previously observed in Na_2O-SiO_2-B_2O_3 melts (Ellsworth, 1994) and, as discussed below, the temperature-dependent changes in boron speciation seem to involve other bulk compositions used in our study, as the boron speciation appears

to affect partitioning of Na and Al between the immiscible liquids.

5. DISCUSSION

5.1. Relationships Between the Stable and Metastable Liquid Immiscibility

One of the goals of our experiments was to determine the compositional phase boundaries between stable and metastable immiscibility, as well as between those and regions of total mixing along the $CaB_2Si_2O_8$-$CaAl_2Si_2O_8$, $CaB_2Si_2O_8$-$NaBSi_3O_8$ and $CaB_2Si_2O_8$-$NaAlSi_2O_6$ joins. The criterion that we used to distinguish between stable (superliquidus) and metastable (quench) immiscibility was gravitational separation of the immiscible liquids into two distinct layers separated by sharp meniscus after few hours in the high-temperature centrifuge. Opaque, turbid glasses were interpreted as products of metastable phase separation at a scale close to the wavelength range of visible light (the Tyndal effect was observed in some of the turbid glasses).

Pseudoternary projections in Figure 4 show the extent of the region of stable liquid immiscibility along the joins. On the $CaB_2Si_2O_8$-$CaAl_2Si_2O_8$ join, the border of stable immiscibility lies between 18 and 25 mol.% of the anorthite component, while on the $CaB_2Si_2O_8$-$NaBSi_3O_8$ join, the border is reached at ~50 mol.% of $NaBSi_3O_8$, and a region of metastable immiscibility stretches much further to the $NaBO_2$-SiO_2 bounding join (Haller et al., 1970).

5.2. Temperature Dependence of the Partition Coefficients

In Figure 6, partition coefficients (D) for the major elements are plotted against reciprocal absolute temperature. Experimental points that refer to the same bulk composition run at different temperatures plot well along linear trend lines. Large scatter observed for D_{Ca} in the series with the danburite bulk (CBS) is probably due to the very low concentrations of CaO in LS and concomitant large analytical uncertainties in the microprobe analyses for CaO in these samples.

Positive and negative slopes of the trend lines reflect, in theory, exothermic or endothermic influences of element transfer between LB and LS. In this respect, the most interesting trends are observed for Al and Na. Bulk compositions that contain both Na and Al (the $CaB_2Si_2O_8$-$NaAlSi_2O_6$ join) show negative slopes on the temperature plots, but the compositions along the danburite-anorthite and danburite-reedmergnerite joins show, on the contrary, trend lines with positive slopes. It should also be noted that D_{Na} and D_{Al} in the NCMBAS-20 composition decrease to 1, and Na becomes more compatible with LS at temperatures below 1100°C. Such trends, together with the direction of isothermal tie lines in Figs. 3 and 4, appear to reflect bonding between Na and Al in the melts, as well as strong effects of the $NaAlO_2$ complexes on the mutual solubility of LB and LS phases. The implications of these trends for the structural chemistry of LB and LS liquids and speciation of boron are discussed below in more detail.

Finally, the plots in Figure 6 demonstrate that for all the elements, compositional variations in D values significantly exceed their variations with temperature. In the next section, we take a closer look at the compositional systematics of D values.

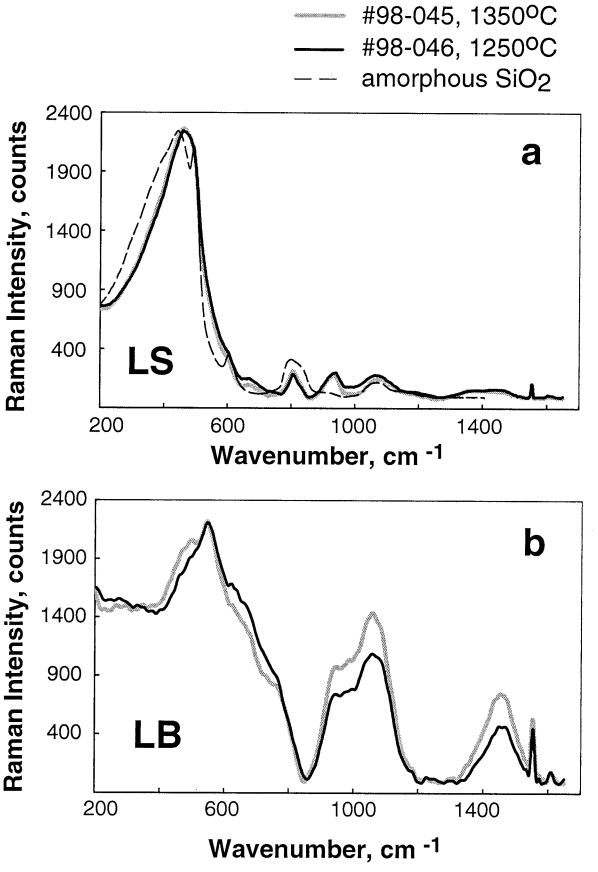

Fig. 5. Raman spectra of glasses in the three-component (CaO-B_2O_3-SiO_2) danburite composition. (a) Silicate-rich liquid (LS) glasses and a spectrum of a-SiO_2 (dashed line). (b) Borate-rich liquid (LB) glasses. The sharp feature at 1550 cm^{-1} is due to molecular O_2 in air. See discussion in the text.

5.3. Variations of the Partition Coefficients With Bulk Composition

The significant scatter of experimental points in temperature plots in Figure 6 requires some explanation. With the exception of Ca in pure danburite (discussed above), the variations appear to be systematic and reflect important chemical changes related to the B-Al and Na-Ca substitutions in the bulk compositions. We tried to correlate the D values with simple chemical parameters of the bulk compositions, or the conjugate liquids. After some trial and error, the best fit was found with the molar values of Si/(Si + Al + B) of the LB, in other words, with the molar fraction of silicon among the network-forming elements of the borate-rich conjugate liquid.

In Figure 7, all the experimental points for D values at T = 1250°C are plotted in logarithmic scale against the Si/(Si + Al + B) parameter. Similar plots can be constructed for 1150 and 1050°C. For all the elements, excluding Al, the points plot tightly along trend lines that radiate from a small region of Si mole fractions 0.52 to 0.55, where all the D values reach 1 (0

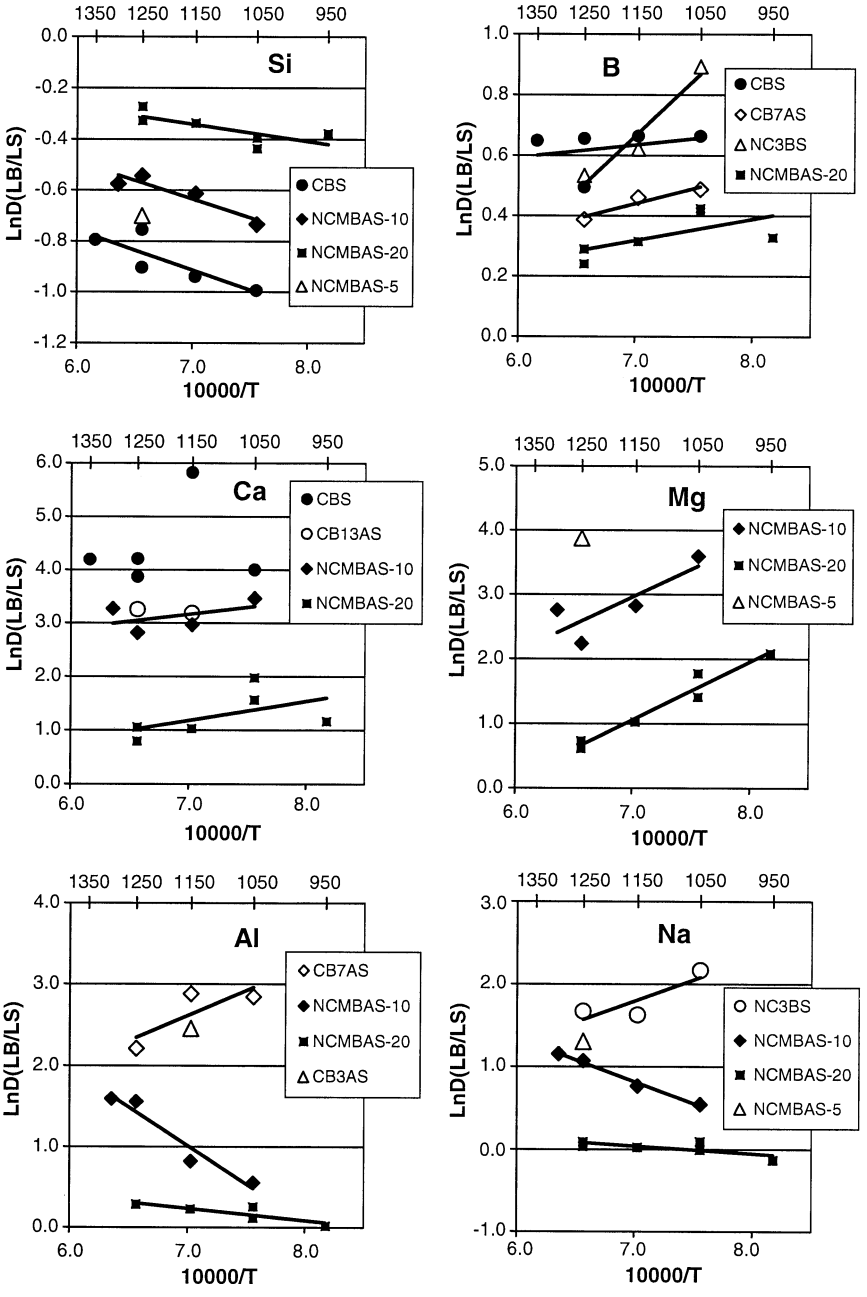

Fig. 6. Natural logarithms of the two-liquid partition coefficients vs. reciprocal absolute temperature with linear fits. Temperature scales in centigrade are shown at the upper borders of the plots. See text for the discussion. LB = borate-rich liquid; LS = silicate-rich liquid.

in the logarithmic scale) and the conjugate liquids merge apparently into a homogeneous melt.

The exception of Al is notable. The points for D_{Al} belong to two groups of bulk compositions, one of which contains sodium (NCMBAS-5, NCMBAS-10, and NCMBAS-20) and the other of which is alkali free (CB7AS and CB13A3S). The points for the sodium-bearing compositions are actually following the trend line of Na, and the values of D_{Na} and D_{Al} are nearly the same. On the other hand, in the alkali-free compositions, D_{Al} has much higher absolute values and plots close to the trend lines of D_{Mg} and D_{Ca}. This is another indication that in sodium-bearing compositions, Na and Al form very strong aluminosilicate complexes with Na-Al mole ratios close to 1, and the complexes may partition between the conjugate LB and LS as a single molecule. This is probably why Na and Al in the alumosilicate bulk compositions show very similar partitioning trends (Figs. 6 and 7).

The correlations of D values with the Si/(Si + Al + B) mole values of LB reflect variable widths of miscibility gaps on the multicomponent joins. The isothermal projections of tie lines

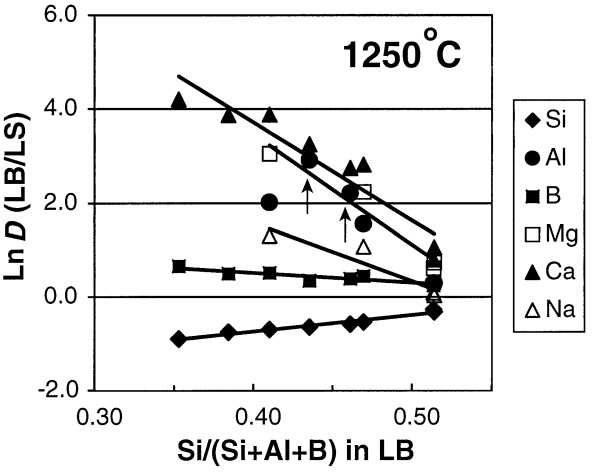

Fig. 7. Natural logarithms of the two-liquid partition coefficients vs. the mole fraction of Si in the sum of network-forming cations of the borate-rich immiscible liquids. Experimental points and linear fits. All the points refer to the runs at 1250°C. Data points for Al in Na-free compositions are marked by arrows. See discussion in the text. LB = borate-rich liquid; LS = silicate-rich liquid.

shown in Figures 3 and 4 demonstrate that the addition of other oxides (especially Na_2O) to the danburite basic composition CBS results in dramatic increase in the SiO_2 content of the conjugate LB liquid and significant narrowing of the miscibility gap. This, however, does not explain why Na and Al change preferences from LB to LS (Fig. 6). Such behaviour is probably due to changes in proportions of trigonal and tetrahedral boron at a fixed bulk boron content, which are discussed in the next section.

5.4. Relationships Between Tetrahedral and Trigonal Boron

Some systematics of the two-liquid element partitioning displayed in Figures 6 and 7 may reflect subtle changes in boron speciation and the proportions of trigonal (BO_3) and tetrahedral (BO_4) groups. Our Raman results for the LB glasses suggest that the proportion of BO_4 species relative to the BO_3 groups in LB increases with falling temperature. This observation is consistent with the results of previous spectroscopic studies of Ca-boroaluminosilicate glasses (Gupta et al., 1985). Such structural changes may also be expected to influence the speciation of water in hydrous borosilicate melts (e.g., Romano et al., 1995).

In alkali silicate melts that contain both aluminium and boron, the latter two cations appear to compete for tetrahedral positions and for the available alkali cations to stabilize their tetrahedral coordination. Raman spectroscopic studies by Konijnendijk and Stevels (1975) and NMR studies by Geisinger et al. (1988) have demonstrated that the progressive addition of Al_2O_3 to M_2O-B_2O_3-SiO_2 glass (M = Na or K) leads to the replacement of borate tetrahedra by aluminate tetrahedra and to stronger preference of boron for trigonal coordination.

The increase in the proportion of tetrahedral boron for a fixed bulk with falling temperature may push some aluminium out of tetrahedral sites and the whole alkali-aluminosilicate complexes from LB to LS. This is probably the reason for the temperature trends of D_{Na} and D_{Al} in the NCMBAS-20 bulk composition demonstrated in Figure 6 and may explain why aluminium and sodium become more soluble in the LS at low temperature, as observed in this complex multicomponent composition.

5.5. Comparisons With Element Partitioning in Silicate-Carbonate Immiscible Systems

Boron and carbon are neighbours in the periodic table and show some similarity with respect to their structural and chemical roles in silicate melts. Like boron, carbon can form trigonal carbonate CO_3 units (Genge et al., 1995), and liquid immiscibility is widespread in silicate-carbonate systems. The immiscibility is believed to be of great petrogenetic importance and responsible for the origin of some types of carbonatites (Hamilton et al., 1979; Bailey, 1993).

Unlike boron, carbon is not a network former, and carbonate melts are totally depolymerised. Carbon is not found in tetrahedral coordination with oxygen (at least at low and moderate pressures). In addition to the carbonate groups, in silicate melts, carbon is partly dissolved in the form of CO_2 molecules (Blank and Brooker, 1994), and the solubility of carbon strongly depends on pressure because of large volume effects of decarbonation reactions.

Two-liquid carbonate-silicate major and trace element partitioning has been the subject of numerous experimental studies (e.g., Hamilton et al., 1989; Kjarsgaard et al., 1995; Jones et al., 1995; Veksler et al., 1998), and the results obtained so far enable some general comparisons between the patterns of two-liquid element partitioning in the carbonate-silicate and borate-silicate immiscible systems to be drawn.

The differences between the two systems are pronounced. First of all, the nature of the silicate-rich conjugate liquid (LS) is very different. Our Raman results have shown that in borosilicate systems, LS is highly polymerised and composed mainly of two network-forming oxides: SiO_2 and B_2O_3. On the other hand, for carbonate-silicate liquid immiscibility, the degree of polymerisation in LS is variable depending on the bulk composition, but more often than not, LS is silica undersaturated and depolymerised. Al_2O_3, the third major network-forming oxide, also shows very different behaviour. It has very low solubility in carbonate-rich immiscible liquids (LC) and demonstrates one of the highest LS/LC partition coefficients, while in case of borate-silicate unmixing, Al_2O_3 either partitions to the depolymerised LB or has nearly equal concentrations in both conjugate liquids.

The behaviour and roles of components that act as network modifiers are also different. Peralkalinity is one of the main driving forces of carbonate-silicate unmixing, and LC-LS immiscibility is not observed in alkali-free systems, such as the CaO-SiO_2-CO_2 join (Lee et al., 1994). Ca and Na partition to LC, while Mg and K are usually more compatible with LS (at least at low pressures). This is not the case in borosilicate systems. The widest LB-LS miscibility gaps are observed in alkali-free systems with divalent alkali earth cations (e.g., CaO-B_2O_3-SiO_2), while in alkaline borosilicate systems, liquid immiscibility is suppressed to subliquidus. Ca and Mg have very high and almost equal LB/LS partition coefficients, while Na,

as discussed above, shows complex behaviour and changes preference from LB to LS with temperature and bulk composition.

In conclusion, borosilicate systems present a peculiar case of liquid immiscibility driven by moderate structural incompatibility between the major network-forming elements. Both conjugate liquids have a strong tendency to polymerisation, but because of the contrasting two-liquid partitioning of network-modifiers, LS is polymerised to a much greater degree than LB. BO_3 and BO_4 units are much more compatible with other network-forming components (SiO_2 and Al_2O_3) than the CO_3 analogues and CO_2 molecules, which do not polymerise at all. As a result, the pattern of two-liquid element partitioning in borosilicate systems is very different from that in carbonate-silicate immiscible systems, and network-modifying cations have different effects on carbonate-silicate and borate-silicate unmixing.

5.6. Chances for Natural Occurrence of Borate-Silicate Liquid Immiscibility and Perspectives for Future Experiments

Some granite pegmatites show strong enrichment in boron (London et al., 1996; Peretyazko et al., 2000), and their parental melts are the closest natural analogues of the LS synthetic compositions. The levels of B_2O_3 concentrations reached in the natural melts are, however, at least several times, if not an order of magnitude, lower than the minimal B_2O_3 saturation limit of 11.7 wt.% detected in the LS in our experiments (Table 3, sample 98-030). This simple consideration alone makes natural occurrences of this particular type of liquid immiscibility very unlikely.

In natural magmatic systems, boron accumulates in residual liquids together with volatiles and other incompatible components. Strong affinity of boron to aqueous magmatic fluids is a clear indication of strong bonds between H_2O and B_2O_3. It is most likely that in natural silicate melts, boron is dissolved in the form of hydrated species, and this has further important implications for the possibility of borate-silicate unmixing. Dry compositions studied in our experiments should be viewed only as a limiting case, first-step approach to boron-rich natural magmatic systems. Experimental studies of pegmatitic, volatile, and B-rich compositions are currently under way (Veksler and Thomas, 2001). One result of the ongoing high-pressure experiments is worth mentioning here. We have run the danburite (CBS) bulk composition with H_2O in a cold-seal, rapid-quench pressure vessel at 900°C and 0.2 GPa and found no signs of the LS-LB immiscibility. A single homogeneous borosilicate glass, wollastonite crystals, and condensates from aqueous vapour were the only phases detected in the run products after quench. Thus, H_2O appears to suppress dramatically the LS-LB unmixing and reduce the chances for this type of liquid immiscibility in natural magmas.

The high-pressure experiment with danburite composition represents another limiting case in which hydrated borosilicate melt coexists with a dilute aqueous fluid. Apart from H_2O, natural B-rich magmatic systems may contain significant amounts of F, Cl, P, and other fluxes that are known to have a limited solubility in aluminosilicate melts and to form immiscible liquids. Relatively simple compositions, similar to those reported here, are not sufficient for adequate modelling of such complex natural systems as granite pegmatites. But they provide important constraints and comparisons to put natural melts into a broader perspective. Although in natural magmas, the generation of Ca-rich borosilicate liquids similar to LB by liquid immiscibility is extremely unlikely, other types of immiscible B-rich melts and fluids are supported by observations in natural melt and fluid inclusions (Peretyazko et al., 2000; Thomas et al., 2000). Experimental modelling of their generation is a task for future studies.

Acknowledgments—We thank Detlef Krausse (BGI, Bayreuth), Dieter Rhede and Oona Appelt (GFZ Potsdam) for their assistance in electron microprobe analyses. Reviews by Richard A. Brooker, Adrian P. Jones, and Claudia Romano helped improve the manuscript.

Associate editor: C. Romano

REFERENCES

Bailey D. K. (1993) Carbonate magmas. *J. Geol. Soc. London* **150,** 637–651.

Blank J. G. and Brooker R. A. (1994) Experimental studies of carbon dioxide in silicate melts: Solubility speciation and stable carbon isotope behavior. In *Volatiles in Magmas,* 30 (eds. M. R. Carroll and J. R. Holloway. Rev. Mineral., 157–186.

Chryssikos G. D., Kamitsos E. I., Patsis A. P., Bitsis M. S., and Karakassides M. A. (1990. *J. Non-Cryst. Solids* **126,** 42.

Dingwell D. B., Knoche R., Webb S. L., and Pichavant M. (1992) The effect of B_2O_3 on the viscosity of haplogranitic melts. *Am. Mineral.* **77,** 457–561.

Dingwell D. B., Pichavant M., and Holtz F. (1996) Experimental studies of boron in granitic melts. In *Boron: Mineralogy, Petrology and Geochemistry,* 33 (eds. E. S. Grew and L. M. Anowitz. Rev. Mineral., 331–386.

Dorfman A. M., Hess K.-U., and Dingwell D. B. (1996) Centrifuge-assisted falling-sphere viscometry. *Eur. J. Mineral.* **8,** 507–514.

Ellsworth S. E.(1994) *Borate and Borosilicate Melts: High Temperature MAS NMR and Fictive Temperature Studies*. M.S. thesis, Stanford University.

Furukawa T. and White W. B. (1981) Raman spectroscopic investigation of sodium borosilicate glass structure. *J. Mater. Sci.* **16,** 2689–2700.

Galeener F. L. (1982) Planar rings in vitreous silica. *J. Non-Cryst. Solids* **49,** 53–62.

Geisinger K. L., Oestrike R., Navrotsky A., Turner G. L., and Kirkpatrick R. J. (1988) Thermochemistry and structure of glasses along the join $NaAlSi_3O_8$-$NaBSi_3O_8$. *Geochim. Cosmochim. Acta* **52,** 2405–2414.

Genge M. J., Jones A. P., and Price G. D. (1995) An infrared and Raman study of carbonate glasses: Implications for the structure of carbonatite magmas. *Geochim. Cosmochim. Acta* **59,** 927–937.

Gibbs G. V. (1982) Molecules as models for bonding in silicates. *Am. Mineral.* **67,** 421–450.

Gupta P. K., Lui M. L., and Bray P. J. (1985) Boron coordination in rapidly cooled and in annealed aluminuim borosilicate glass fibres. *J. Am. Ceram. Soc.* **68,** C-82.

Haller W., Blackburn D. H., Wagstaff F. E., and Charles R. J. (1970) Metastable immiscibility surface in the system Na_2O-B_2O_3-SiO_2. *J. Am. Ceram. Soc.* **1,** 34–39.

Hamilton D. L., Freestone I. C., Dawson J. B., and Donaldson C. H. (1979) Origin of carbonatites by liquid immiscibility. *Nature* **279,** 52–54.

Hamilton D. L., Bedson P., and Esson J. (1989) The behaviour of trace elements in the evolution of carbonatites. In *Carbonatites: Genesis and Evolution* (ed. K Bell), 405–427. Unwin Hyman, London.

Jones J. H., Walker D., Picket D. A., Murrel M. T., and Beattie P. (1995) Experimental investigations of the partitioning of Nb, Mo, Ba, Ce, Pb, Ra, Th, Pa and U between immiscible carbonate and silicate liquids. *Geochim. Cosmochim. Acta* **59,** 1307–1320.

Konijnendijk W. L. and Stevels J. M. (1975) The structure of borosilicate glasses studied by Raman scattering. *J. Non-Cryst. Solids* **20,** 193–224.

Kjarsgaard B. A., Hamliton D. L., and Peterson T. D. (1995) Peralkaline nephelinite/carbonatite liquid immiscibility: Comparison of phase compositions in experiments and natural lavas from Oldoinyo Lengai. In *Carbonatite Volcanism: Oldoinyo Lengai and Petrogenesis of Natrocarbonatites* (eds. K. Bell and J. Keller), 163–190. Springer-Verlag, Berlin, Germany.

Lee W.-J., Wyllie P. J., and Rossman G. R. (1994) CO_2-rich glass, round calcite crystals and no liquid immscibility in the system CaO-SiO_2-CO_2 at 2.5 GPa. *Am. Mineral.* **79,** 1135–1144.

Leeman W. P. and Sisson W. B. (1996) Geochemistry of boron and its implications for crustal and mantle processes. In *Boron: Mineralogy, Petrology and Geochemistry*, 33 (eds. E. S. Grew and L. M. Anowitz. Rev. Mineral., 645–708.

Levin E. M., Robbins C. R., and McMurdie H. F. (1964. Phase Equilibria Diagrams Vol. 1. American Ceramic Society, Westerville, OH.

London D., Morgan IV G. B., and Wolf M. B. (1996) Boron in granitic rocks and their contact aureoles. In *Boron: Mineralogy, Petrology and Geochemistry*, 33 (eds. E. S. Grew and L. M. Anowitz. Rev. Mineral., 299–330.

McMillan P. F. (1984) Structural studies of silicate glasses and melts—Applications and limitations of Raman spectroscopy. *Am. Mineral.* **69,** 622–644.

Morey G. W. and Ingerson E. (1937) The melting of danburite, a study of liquid immiscibility in the system CaO-B_2O_3-SiO_2. *Am. Mineral.* **22,** 37–47.

Mysen B. O., Virgo D., and Scarfe C. M. (1980) Relations between the anionic structure and viscosity of silicate melts—A Raman spectroscopic study. *Am. Mineral.* **65,** 690–710.

Peretyazko I. S., Prokof'ev V. Yu., Zagorskii V. E., and Smirnov S. Z. (2000) Role of boric acid in the formation of pegmatite and hydrothermal minerals: Petrologic consequences of sassolite (H_3BO_3) discovery in fluid inclusions. *Petrology* **8,** 214–237.

Pichavant M. (1987) Effects of B and H_2O on liquidus phase relations in the haplogranite system at 1 kbar. *Am. Mineral.* **72,** 1056–1070.

Pichavant M., Kontak D. J., Briqueu L., Herrera J. V., and Clark A. H. (1988) The Miocene-Pliocene Macusani volcanics, SE Peru II. Geochemistry and origin of a felsic peraluminous magma. *Contrib. Mineral. Petrol.* **100,** 325–338.

Rockett T. J. and Forster W. R. (1965) Phase relations in the system SiO_2-B_2O_3. *J. Am. Ceram. Soc.* **48,** 75–80.

Romano C., Dingwell D. B., and Hess K.-U. (1995) The effect of boron on the speciation of water in haplogranitic melts. *Periodico di Mineralogia* **64,** 413–431.

Scholze H. (1988) *Glas*. Springer, Berlin, Germany (in German).

Seifert F. A., Mysen B. O., and Virgo D. (1982) Three-dimensional network structure of quenched melts (glass) in the systems SiO_2-$NaAlO_2$, SiO_2-$CaAl_2O_4$ and SiO_2-$MgAl_2O_4$. *Am. Mineral.* **67,** 696–717.

Thomas R., Webster J. D., and Heinrich W. (2000) Melt inclusions in pegmatite quartz: Complete miscibility between silicate melts and hydrous fluids at low pressure. *Contrib. Mineral. Petrol.* **139,** 394–401.

Veksler I. V., and Thomas R.(2001) Phase equilibria, mineral-melt and fluid-melt element partitioning in the haplopegmatite system. In *Eleventh Annual V. M. Goldschmidt Conference* (Abstract #3190, LPI Contribution No. 1088), Lunar and Planetary Institute, Houston, TX (CD-ROM).

Veksler I. V., Petibon C., Jenner G. A., Dorfman A. M., and Dingwell D. B. (1998) Trace element partitioning in immiscible silicate-carbonate liquid systems: An initial experimental study using a centrifuge autoclave. *J. Petrol.* **39,** 2095–2104.

Zotov N., Ebbsjö I., Timpel D., and Keppler H. (1999) Calculation of Raman spectra and vibrational properties of silicate glasses: Comparison between $Na_2Si_4O_9$ and SiO_2 glasses. *Phys. Rev. B* **60,** 6383–6397.